Comparative Analysis of Battery State of Charge Estimation Methods

Ali Margal[1*], *Soukaina* El Daoudi[1], *Abdelmounaim* Khallouq[1], and *Asma* Karama[1]

[1]A2(IS) Research Team, Physics Department, Faculty of Sciences Semlalia, Cadi Ayyad University, Marrakesh, Morocco.

Abstract. Lithium-ion batteries are widely used in electric vehicles, buses, etc., due to their high-power density, long lifespan, and high energy density. To efficiently manage energy in these vehicles, a Battery Management System (BMS) is crucial. A critical parameter for the BMS is the State of Charge (SoC), which indicates the available charge in the battery and ensures its operational range. This paper presents three methods for estimating SoC: the extended Kalman filter (EKF), the adaptive Luenberger observer (ALO), and a neural network model employing nonlinear auto-regressive with eXogenous inputs (NARX). These methods are evaluated under the LA92 driving cycle using metrics like Root Mean Square Error (RMSE) to assess their performance. Results show that the NARX model achieves the highest accuracy with an RMSE of 0.33%, followed by the EKF with 5.34% and finally the ALO with 5.94%. These findings indicate that all three methods are acceptable, and the proposed NARX model shows superior performance. With the NARX model exhibiting superior performance in SoC estimation for electric vehicle applications.

1 Introduction

Due to the environmental effect of transportation emissions, in particular greenhouse gases, the market industry is increasingly moving towards electric vehicles (EVs). However, these vehicules face significant challanges in power storage [1], which directly affects their autonomy and performance. Among various battery technologies used in EVs, lithium-ion batteries remain the most popular in the market because of their high energy and power density, low self-discharge rate, light weight, and long lifespan. Nevertheless, their cost remains expensive [2, 3]. The State of Charge (SoC) indicates the amount of charge stored in the battery that can be used. However, there is no sensor capable of directly measuring the SoC, necessitating the use of reliable estimation techniques. Accurate SoC estimation is crucial for determining the remaining charge in batteries and, consequently, the vehicle's operational range.

Estimation methods can be classified into three categories [4], the first one comprises direct measurement techniques, including open circuit voltage (OCV), Coulomb counting (CC), and electrochemical impedance spectroscopy (EIS). The OCV method is less sensitive to measurement errors, it requires considerable time for the battery to reach the equilibrium state, which depends on several factors of the battery such as temperature, hysteresis effect, construction material, etc. This limits the application of this method; [5]. CC is simple

* Corresponding author : a.margal.ced@uca.ac.ma

to implement; however, it can be inaccurate due to sensor noise and current measurement influenced by sensor noise [6]. However, EIS offers high precision, although it is expensive and complex to implement, and requires knowledge of electrochemical modeling [7].

The second class consists of model-based methods. These include Kalman Filters (KF) and their extended versions, widely adopted for their acceptable accuracy [8]. Nonetheless, they require noise characterization and are sensitive to initial conditions. Non-linear observers provide flexibility and accuracy with non-linear systems but are susceptible to instability and chattering phenomenon. On the other hand, H_∞ filters are robust but complex, relying on multiple parameters of the battery [9].

The third group is data-driven methods [10], known as artificial intelligence approaches, treat the battery model as a black box, using inputs such as current, voltage, and temperature to predict SoC and voltage. Among these techniques, neural networks with their different types are characterized by high accuracy, while fuzzy logic provides good nonlinear prediction capability[11]. Whereas support vector machines (SVM) yield high precision [12]. However, these techniques often require significant computational resources and extensive training data.

This work investigates three estimation techniques for battery state of charge in electric vehicles: the Extended Kalman Filter, the Adaptive Luenberger Observer, and the NARX neural network model.The battery is designed using Thevenin model presentd in [13], while the performance of the methods is evaluated using metrics like mean square error(MSE), root mean square error (RMSE) and mean absolute error (MAE) metrics.

The paper is organized as follows: Section 2 introduces battery modeling and parameter identification. Section 3 details the estimation methods used in this study. Section 4 presents the application and discussion of the simulation results. Finally, Section 5 concludes the paper.

2 Methodology and Materials

2.1 Battery modeling

Various types of battery models can represent the battery's non-linear behavior [3]. Electrochemical models provide a strong approximation, except that they are complex to construct and require expertise in electrochemistry, which limits their implementation. On the other hand, equivalent electric circuit models (EECM) are more widely used for SOC estimation due to their acceptable accuracy and simplicity of implementation [14]. Among EECM models, the Thevenin model remains the most popular. It accurately models the Li-ion diffusion behavior in battery cells using parallel RC branches. While increasing the number of RC branches can improve the model's accuracy in representing battery dynamics, nevertheless, this increases the complexity of estimating the model parameters. Figure 1 present the proposed Thevenin model which called Dual polarization,which is characterized by 2 RC branches.

Based on Kirchhoff's laws [15], the terminal voltage is expressed by:

$$V_T(t) = V_{\text{oc}}(t) - R_0 I_b(t) - v_1(t) - v_2(t) \tag{1}$$

The current flowing through the capacitor of the j-th branch by:

$$i_{C_j} = C_j \frac{dv_j(t)}{dt} = I_b - i_{R_j}(t) \quad \text{where} \quad j \in \{1, 2\} \tag{2}$$

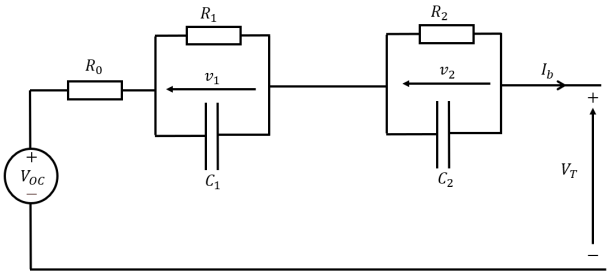

Figure 1. Dual polarization model [16]

Developing equation 2:

$$\frac{dv_j(t)}{dt} = \frac{1}{C_j} I_b - \frac{v_j(t)}{R_j C_j} \quad \text{where} \quad j \in \{1, 2\} \tag{3}$$

R_j, C_j and v_j are respectively the resistance, capacitance and voltage of the j-th branch, R_0 is the internal resistance. I_b represents the current of the battery.

The state of charge is the amount of charge stored in the battery. Which is the ratio of the remaining capacity in the storage unit to the total capacity that the battery can support, which can be represented by :

$$SoC(t) = \frac{C_{remaining(t)}}{C_{total}} \tag{4}$$

The State of Charge (SoC) estimation using the Coulomb Counting (CC) method can be expressed by the following equation :

$$\mathrm{SoC}(t) = \mathrm{SoC}(t_0) - \frac{\eta}{Q_{\mathrm{rated}}} \int_{t_0}^{t} I(t)\, dt \tag{5}$$

CC method is based on the principle of integrating the current flowing in the battery for a given time, divided by the battery's rated charge capacity Q_{rated}. As illustrated in equation 5, $SoC(t)$ and $SoC(t_0)$ denote present and initial SoC values, respectively. $I_b = \eta I$, where η represents the coulombic efficiency, which accounts for the portion of the current that is available after dissipation due to the chemical reactions occurring inside the battery when it is charged or discharged. Generally, the value of η ranges from 0.9 to 1, depending on the temperature and charging rates.

In discrete time the equations (1), (3), (5) can be written respectivley as :

$$V_{T[k]} = V_{\mathrm{oc}[k]} - R_0 I_{b[k]} - v_{1[k]} - v_{2[k]} \tag{6}$$

$$v_{j[k+1]} = e^{\left(-\frac{\Delta t}{\tau_j}\right)} \cdot v_{j[k]} + \frac{1}{C_j} \cdot I_{b[k]} \tag{7}$$

where $j \in \{1, 2\}$ and $\tau_j = R_j C_j$

$$\mathrm{SoC}_{[k+1]} = \mathrm{SoC}_{[k]} - \frac{\eta}{Q_{\mathrm{rated}}} I_{[}b_{[k]}] \cdot \Delta t \tag{8}$$

Δt is the simple time. V_{oc} is the open-circuit voltage.

Using equations (6)–(8), the state space model can be expressed as shown below :

$$\begin{cases} x_{[k+1]} = A_d x_{[k]} + B_d u_{[k]} + \omega_{[k]} \\ y_{[k]} = [0 - 1 - 1] x_k + V_{\mathrm{oc}[k]} + D_d u_{[k]} + \nu_{[k]} \end{cases} \tag{9}$$

Where : $x_{[k]} = [SoC_{[k]}\ v_{1[k]}\ v_{2[k]}]^T$ is the state space vector. Input $u_{[k]}$ is battery current $I_{b[k]}$, output $y_{[k]}$ is the terminal voltage $V_{T[k]}$, $\omega_{[k]}$ is the process noise affecting the system state and $\nu_{[k]}$ is the measurement noise.

$$A_d = \begin{pmatrix} 1 & 0 & 0 \\ 0 & e^{-\frac{\Delta t}{\tau_1}} & 0 \\ 0 & 0 & e^{-\frac{\Delta t}{\tau_2}} \end{pmatrix}, B_d = \begin{pmatrix} -\frac{\eta \Delta t}{Q_{\text{rated}}} \\ R_1(1 - e^{-\frac{\Delta t}{\tau_1}}) \\ R_2(1 - e^{-\frac{\Delta t}{\tau_2}}) \end{pmatrix}, D_d = -R_0$$

2.2 Parameter identification

Table 1 presents the battery data sheet, which includes the nominal capacity and voltage, the lower and upper cut-off voltages, as well as the continuous charge and discharge currents. These data were obtained using a Digatron firing circuit universal battery tester channel. The battery was tested using the Hybrid Pulse Power Characterization (HPPC) method to approximate the battery parameters and establish their relationship with SoC factor[17, 18]. Based

Table 1. Battery Parameters [18]

Parameter	Value
Nominal Capacity	5000 mAh
Nominal Voltage	3.7 V
Upper cut-off Voltage	4.2 V
Lower cut-off Voltage	2.8 V
Continuous charge current	4.2 V, 50 mA
Continuous discharge current	2.8 V, 20 mA

on the findings outlined in [19], it is evident that a non-linear relationship exists between SoC and V_{oc}, as well as with battery parameters R_0, R_1, C_1, R_2, and C_2.

The 5th-order polynomial function employed to approximate the relationship between SoC and each parameter, is expressed as follows:

$$f(\text{SoC}) = a_0 + a_1\text{SoC} + a_2\text{SoC}^2 + a_3\text{SoC}^3 + a_4\text{SoC}^4 + a_5\text{SoC}^5 \tag{10}$$

The Matlab Curve Fitting Toolbox is used to obtain the coefficients given in Table 2

Table 2. Polynomial coefficients

Parameter	a_0	a_1	a_2	a_3	a_4	a_5
R_0 (Ω)	0.0047	-0.0492	0.2727	-0.6345	0.6467	-0.2389
R_1 (Ω)	0.0005	-3.0e4	1.3e4	-2.2e4	1.4e4	-3.0e4
C_1 (F)	1.659e4	0.5195	-2.5661	5.2359	-4.7580	1.5987
R_2 (Ω)	0.0005	-0.0010	0.0066	-0.0170	0.0184	-0.0071
C_2 (F)	1.722e5	5.703e5	-3.3852	8.1916e5	-8.6966e5	3.3494e5
V_{oc} (V)	3.1978	5.0650	-18.3261	32.1540	-25.8096	7.9186

3 SoC estimation methods

The precise value of the State of Charge (SoC) factor is critical for effective energy management. It is one of the essential coefficients provided to the Battery Management System (BMS) to safeguard the battery against overcharging and deep discharging, thereby ensuring

a longer lifespan, minimizing characteristic degradation, providing a reliable estimate of the electric vehicle's operating range[20]. In this section, three estimation methods will be developed: a discrete-time Extended Kalman Filter (EKF), a discrete-time adaptive Luenberger Observer (ALO), and a recurrent neural network-based Nonlinear Auto-regressive Exogenous (NARX) model. Figure 2 illustrates the description of the work. The battery modeling is based on the Thevenin model.

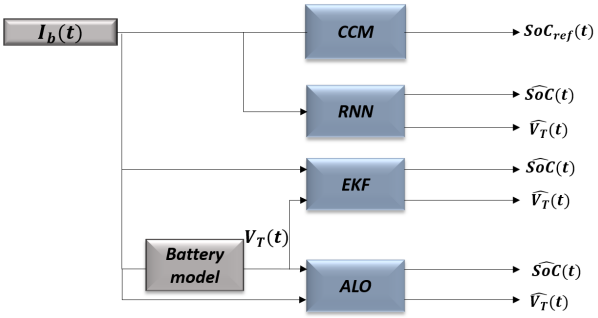

Figure 2. Model architecture for SOC estimation methods

3.1 Extended Kalman Filter (EKF) method

The Kalman filter is widely used for estimation in linear systems. However, for nonlinear and time-varying systems, the Extended Kalman Filter (EKF) is required. it's accounts for system uncertainties and measurement noise[21]. The EKF algorithm consists of three steps:

Step 0: Initialization

- $\hat{\mathbf{x}}_0^+ \leftarrow$ initial state
- $\mathbf{P}_0^+ \leftarrow$ initial error covariance

Step 1: A-priori prediction

- $\hat{\mathbf{x}}_{[k]}^- = \mathbf{A}_d \hat{\mathbf{x}}_{[k-1]}^+ + \mathbf{B}_d \mathbf{u}_{[k-1]}$
- $\mathbf{P}_{[k]}^- = \mathbf{A}_d \mathbf{P}_{[k-1]}^+ \mathbf{A}_d^T + \mathbf{Q}$

Step 2: Update Step

- $\mathbf{K}_{[k]} = \mathbf{P}_{[k]}^- \mathbf{C}_x^T (\mathbf{C}_x \mathbf{P}_{[k]}^- \mathbf{C}_x^T + \mathbf{R})^{-1}$
- $\hat{\mathbf{x}}_{[k]}^+ = \hat{\mathbf{x}}_{[k]}^- + \mathbf{K}_{[k]} (\mathbf{y}_{[k]} - \mathbf{C}_x \hat{\mathbf{x}}_{[k]}^-)$
- $\mathbf{P}_{[k]}^+ = (I - \mathbf{K}_{[k]} \mathbf{C}_x) \mathbf{P}_{[k]}^-$

$\hat{\mathbf{x}}_{[k]}^+$ and $\mathbf{P}_{[k]}^-$ are, respectively, the prior values of $\mathbf{x}_{[k]}$ and the covariance matrix at instant $[k]$, $\mathbf{K}_{[k]}$ is the Kalman gain at time k, $\mathbf{Q}$ and $\mathbf{R}$ are, respectively, the covariance matrices of process and measurement noise, i.e. the choice of that matrix influences the estimation perfermance [22].
As noted above, there is a non-linear dependency between SoC and V_{oc}, therefore $\mathbf{C}_x$ is the partial derivative (Jacobian matrice) of the non-linear output function, hence :

$$\mathbf{C}_x = \frac{\partial V_{T[k]}}{\partial \text{SoC}_{[k]}, v_{1[k]}, v_{2[k]}} = \left[\frac{\partial V_{\text{oc(SoC[k])}}}{\partial \text{SoC}_{[k]}} - 1 - 1 \right] \tag{11}$$

3.2 Adaptive Luenberger observer method :

The Luenberger observer is designed to estimate states for linear systems. For nonlinear and time-varying systems, an extended Luenberger observer was developed. This method is based on minimizing the mean square error using the stochastic gradient approach developed by Widrow [23]. The observer gain is adapted iteratively to make the error reaching the minimum value, the algorithm of this method is given as follows:

Step 0: Initialization

- $\hat{\mathbf{x}}_1^- \leftarrow$ initial state
- $\frac{\partial \hat{\mathbf{x}}_0}{\partial \mathbf{K}} \leftarrow$ initial partial derivative
- $\mathbf{K}_0 \leftarrow$ initial the gain

Step 1: Update and prediction

- $\mathbf{K}_{[k]} = \mathbf{K}_{[k-1]} + 2\lambda(y_{[k]} - \mathbf{C}_x\hat{\mathbf{x}}_{[k]}^-)\mathbf{C}_x\mathbf{A}_d\frac{\partial \hat{\mathbf{x}}_{[k-1]}}{\partial \mathbf{K}}$
- $\hat{\mathbf{x}}_{[k]} = \mathbf{A}_d\hat{\mathbf{x}}_{[k]} + \mathbf{B}_d\mathbf{u}_{[k-1]} + \mathbf{K}_{[k]}(\mathbf{y}_{[k]} - \mathbf{C}_x\hat{\mathbf{x}}_{[k]}^-)$
- $\frac{\partial \hat{\mathbf{x}}_{[k]}}{\partial \mathbf{K}} = (\mathbf{I}_n - \mathbf{K}_{[k]}\mathbf{C}_x)\mathbf{A}_d\frac{\partial \hat{\mathbf{x}}_{[k-1]}}{\partial \mathbf{K}} + (y_{[k]} - \mathbf{C}_x\hat{\mathbf{x}}_{[k]}^-)$

λ and $\frac{\partial \mathbf{x}}{\partial \mathbf{K}}$ represent respectively the learning rate and the partial derivative of $\hat{\mathbf{x}}$, n is the dimension of state space system model and $\mathbf{K}_k$ is the observer gain. The other variables are those described in the previous paragraph.

3.3 Recurrent neural network

The Non-linear Auto-Regressive with eXogenous inputs (NARX) model is a type of neural network. This process is classified as an artificial intelligence techniques, such as fuzzy logic, genetic algorithms, and support vector machines, NARX is a class of dynamic neural networks designed to process sequential data[24]. In this work, the model is based on historical and current battery data to describe the nonlinear system. It takes as input actual and previous values of current ($\mathbf{I}_{\mathbf{b}k}, \ldots, \mathbf{I}_{\mathbf{b}k-nu}$) and the previous outputs($\hat{\mathbf{SoC}}_{k-1} \ldots \hat{\mathbf{SoC}}_{k-ny}$) and ($\hat{\mathbf{V}}_{Tk-1} \ldots \hat{\mathbf{V}}_{Tk-ny}$) until *nu* and *ny* (the orders of delay in input and output, respectively), to enhance accuracy and prevent the accumulation of errors. The output vector is the current state of charge $\hat{\mathbf{SoC}}_k$ and the terminal voltage $\hat{\mathbf{V}}_{\mathbf{T}k}$. Figure 3 shows a schematic of the proposed model.

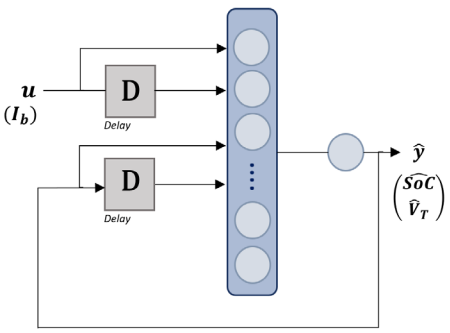

Figure 3. Description of Recurrent Neural Network Modelused

After several tests the Table 3 presents the hyperparameters and the optimisation algorithm used to train the NARX model.

Table 3. Hyperparameters of RNN

Hyperparameter	Description
Learning Rate	0.001
Hidden Units	5
Hidden Layer	1
Activation Function	ReLU, Tanh
Delay Parameter D	2
Optimizer	Adam
Loss Function	MSE
Epochs	1000

4 Results and discussion

The Turnigy Graphene 5000mAh 3S 65C Li-Polymer battery was tested using the LA 92 driving cycle and other cycles listed in [18]. LA 92, developed by California Air Resources Board, is a dynamometer-based driving program for light vehicles. This cycle, lasting 7478 seconds (2.08h), serves as the basis for analysis. Figure 4 shows the current profile for the LA 92 cycle, drawn by the vehicle motor, while Figure 5 presents the corresponding battery voltage.

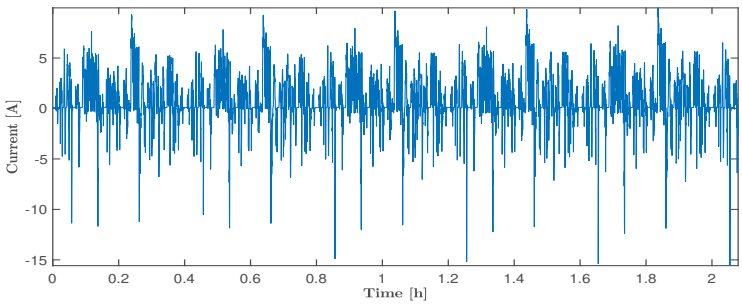

Figure 4. Current of the battery

During acceleration, the battery discharges, resulting in a positive current and voltage drop. When energy extraction stops, the current reverses, represented by a negative current indicating recharging, and the voltage rises. However, since discharge time is typically longer than charge time, the voltage gradually drops with oscillations, as shown in Figure 5.

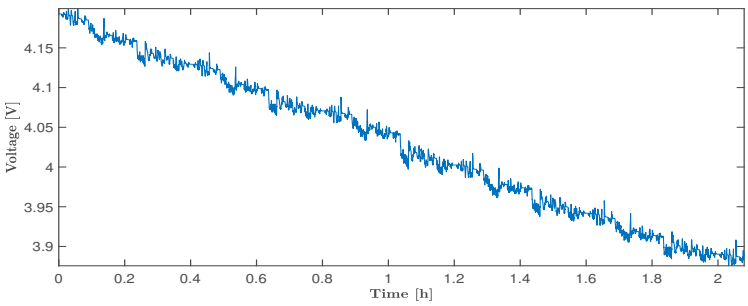

Figure 5. Terminal voltage of the battery

To evaluate the accuracy of the different methods, the RMSE (Root Mean Square Error), MSE (Mean Square Error), and MAE (Mean Absolute Error) criteria are used.

With :

$$\text{MSE} = \frac{1}{N}\sum_{k=1}^{N}(\text{SoC}_k - \hat{\text{SoC}}_k)^2 \tag{12}$$

$$\text{RMSE} = \sqrt{\text{MSE}} = \sqrt{\frac{1}{N}\sum_{k=1}^{N}(\text{SoC}_k - \hat{\text{SoC}}_k)^2} \tag{13}$$

$$\text{MAE} = \frac{1}{N}\sum_{k=1}^{N}|\text{SoC}_k - \hat{\text{SoC}}_k| \tag{14}$$

N is the number of samples.

Figure 6 compares the estimated terminal voltages using various methods namely ALO, EKF and NARX. The zoomed-in section on the right emphasises the initial part of the estimation process, showing that methods based on the Dual Polarization model converge after a short period, while the RNN initially exhibits oscillations before converging. In general, all three methods closely approximate the actual voltage of the battery.

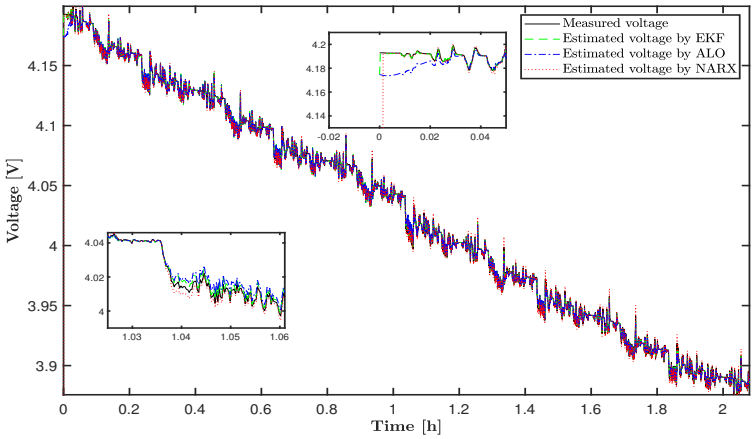

Figure 6. Comparison of Terminal Voltage Estimation

In the second zoom-in on the left, it is evident that the voltage estimated by the NARX model shows a bias compared to the reference. In contrast, the EKF and ALO methods closely align with the reference. However, in a short period of time, the estimation algorithm was able to overcome the deviation, as shown in Figure 6, Figure 7 illustrates the relative voltage error, highlighting a variation margin of 0.01V. In the zoomed-in view, it is clear that the error generated by the RNN model remains the closest to zero, which is prominently detailed in Table 4.

Table 4. Evaluation of Voltage Estimation

Method	MSE	RMSE	MAE
KF	1.4377×10^{-6}	5.349×10^{-1}	7.4787×10^{-4}
ALO	2.6794×10^{-6}	5.948×10^{-1}	8.9792×10^{-4}
NARX	6.5442×10^{-7}	3.3288×10^{-2}	4.8831×10^{-4}

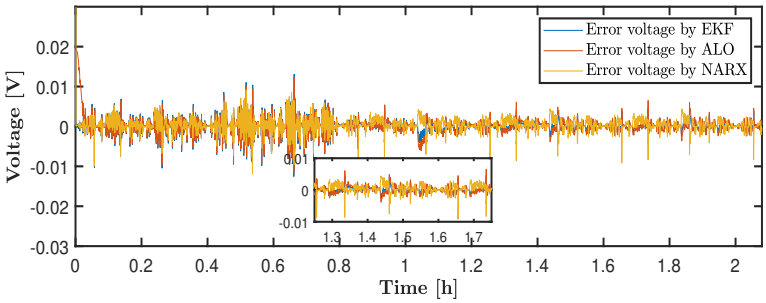

Figure 7. Relative Error of Voltage

Figure 8 shows the comparison between the estimated SoC values and its actual value using the CC method, which is chosen as the reference. As mentioned previously, the CC method is not suitable for use in real-life conditions because it requires the exact initial value of the SoC , which is often not readily available. The absence of this value introduces an accumulation of errors, leading to an inaccurate SoC. However, the CC method can be retained as an ideal reference for the estimation if the initial SoC value is known.

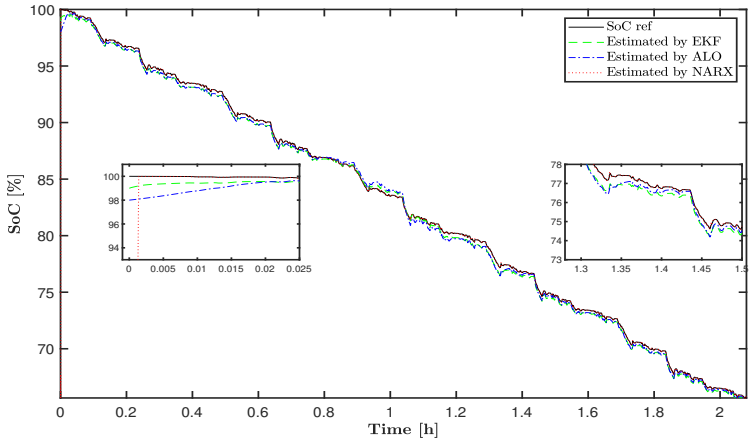

Figure 8. Comparison of SoC

Focusing on the initial part illustrated by the zoom on the left of Figure 8, the NARX model starts with a small oscillation before converging fast. In the other hand, the other two estimators converge more slowly than the proposed RNN with no oscillations. In the second zoom-in on the right, it is observed that the NARX model closely matches the reference voltage, indicating high accuracy in its estimation. Conversely, the other algorithms exhibit a small deviation from the reference. However, these deviations remain within acceptable limits, demonstrating that the NARX model offers outstanding accuracy.

Figure 9 clearly illustrates the errors associated with the three evaluated methods. The proposed model achieves the highest accuracy, evidenced by an MSE value of 1.1081×10^3, as shown in Table 5. The Extended Kalman Filter (EKF) follows with an MSE of 3.3288×10^2, demonstrating relatively good performance. The Ant Lion Optimizer (ALO) method has the highest error, with an MSE of 2.3208×10^2. This comparison highlights the superior accuracy of the proposed model, followed by EKF and then ALO.

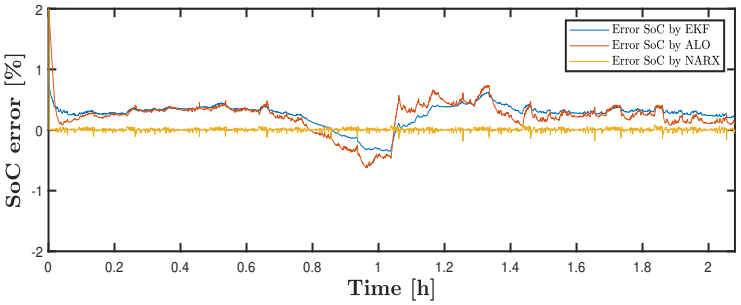

Figure 9. Relative Error of SoC

Table 5. Evaluation of SoC Estimation

Method	MSE	RMSE	MAE
KF	2.8612×10^{-1}	5.349×10^{-1}	4.4996×10^{-1}
ALO	3.5379×10^{-1}	5.948×10^{-1}	4.9046×10^{-1}
NARX	1.1081×10^{-3}	3.3288×10^{-2}	2.3208×10^{-2}

5 Conclusion

State of charge estimation in electric vehicles is a crucial process for energy management, requiring robustness against measurement noise from sensors and other influencing parameters. In this work, three state of charge estimation methods are presented to show and compare their performances. Undoubtedly, the NARX model demonstrates superior accuracy consistently across all operational phases. However, this model requires comprehensive data describing all operational points of the battery to be effective. In contrast, the Extended Kalman Filter (EKF) and Adaptive Luenberger Observer (ALO) rely on the battery's electrical model, which spans the entire operating range.

References

[1] Habib, S., Ali, M., Khan, M. A. (2021). A review on electric vehicle battery technologies, state of charge estimation and management systems. *Energy Reports*, 7, 105-123.

[2] W. Liu, T. Placke, K.T. Chau, Energy Reports **8**, 4058–4084 (2022)

[3] G. Pravallika, P. Sujatha, P. Bharath Kumar, Materials Today: Proceedings (2023)

[4] A. Singh, K. Pal, C.B. Vishwakarma, e-Prime-Advances in Electrical Engineering, Electronics and Energy **6**, 100328 (2023)

[5] Q.-Q. Yu, R. Xiong, L.-Y. Wang, C. Lin, Chinese Journal of Mechanical Engineering **31**, 1–8 (2018)

[6] K. Movassagh, A. Raihan, B. Balasingam, K. Pattipati, Energies **14**(14), 4074 (2021)

[7] U. Westerhoff, T. Kroker, K. Kurbach, M. Kurrat, Journal of Energy Storage **8**, 244–256 (2016)

[8] P. Shrivastava, P.A. Naidu, S. Sharma, B.K. Panigrahi, A. Garg, Journal of Energy Storage **64**, 107159 (2023)

[9] B. Xia, Z. Zhang, Z. Lao, W. Wang, W. Sun, Y. Lai, M. Wang, Energies **11**(6), 1481 (2018)

[10] D.N.T. How, M.A. Hannan, M.S. Hossain Lipu, P.J. Ker, IEEE Access **7**, 136116-136136 (2019)

[11] D. Saji, P.S. Babu, K. Ilango, in *2019 4th International conference on recent trends on electronics, information, communication & technology (RTEICT)* (IEEE, 2019), pp. 948–952

[12] J. Li, M. Ye, W. Meng, X. Xu, S. Jiao, IEEE Access **8**, 195398–195410 (2020)

[13] You, H. W., Bae, J. I., Cho, S. J., Lee, J. M., & Kim, S. H. (2018). Analysis of equivalent circuit models in lithium-ion batteries. *AIP Advances*, 8(12).

[14] X. Ding, D. Zhang, J. Cheng, B. Wang, P.C.K. Luk, Applied Energy **254**, 113615 (2019)

[15] B.L. Theraja, *Basic Electronics: Solid State* (S. Chand Publishing, 2006)

[16] Z. Zhang, L. Jiang, L. Zhang, and C. Huang, "State-of-charge estimation of lithium-ion battery pack by using an adaptive extended Kalman filter for electric vehicles," *Journal of Energy Storage*, vol. 37, pp. 102457, 2021. doi: https://doi.org

[17] Z. Li, X. Shi, M. Shi, C. Wei, F. Di, H. Sun, in *2020 Asia Energy and Electrical Engineering Symposium (AEEES)* (IEEE, 2020), pp. 753–757

[18] P. Kollmeyer, M. Skells, Mendeley Data **1**, 10–17632 (2020)

[19] X. Lai, W. Gao, Y. Zheng, M. Ouyang, J. Li, X. Han, L. Zhou, Electrochimica Acta **295**, 1057–1066 (2019)

[20] X. Han, L. Lu, Y. Zheng, X. Feng, Z. Li, J. Li, M. Ouyang, ETransportation **1**, 100005 (2019)

[21] G. Welch, G. Bishop, Chapel Hill, NC, USA (1995)

[22] Z. Zhang, L. Jiang, L. Zhang, C. Huang, Journal of Energy Storage **37**, 102457 (2021)

[23] Y. Wang, J. Tian, Z. Sun, L. Wang, R. Xu, M. Li, Z. Chen, Renewable and Sustainable Energy Reviews **131**, 110015 (2020)

[24] S. Bockrath, A. Rosskopf, S. Koffel, S. Waldhör, K. Srivastava, V.R.H. Lorentz, in *IECON 2019-45th Annual Conference of the IEEE Industrial Electronics Society* (IEEE, 2019), vol. 1, pp. 2507–2511